Efficient Tensor Network *Ansatz* for High-Dimensional Quantum Many-Body Problems

Timo Felser,[1,2,3] Simone Notarnicola,[2,3,4] and Simone Montangero[2,3,4]
[1]*Theoretische Physik, Universität des Saarlandes, D-66123 Saarbrücken, Germany*
[2]*Dipartimento di Fisica e Astronomia "G. Galilei", Università di Padova, I-35131 Padova, Italy*
[3]*INFN, Sezione di Padova, Via Marzolo 8, I-35131 Padova, Italy*
[4]*Padua Quantum Technology Research Center, Università di Padova, I-35131 Padova, Italy*

(Received 26 November 2020; accepted 25 February 2021; published 29 April 2021)

We introduce a novel tensor network structure augmenting the well-established tree tensor network representation of a quantum many-body wave function. The new structure satisfies the area law in high dimensions remaining efficiently manipulatable and scalable. We benchmark this novel approach against paradigmatic two-dimensional spin models demonstrating unprecedented precision and system sizes. Finally, we compute the ground state phase diagram of two-dimensional lattice Rydberg atoms in optical tweezers observing nontrivial phases and quantum phase transitions, providing realistic benchmarks for current and future two-dimensional quantum simulations.

DOI: 10.1103/PhysRevLett.126.170603

Recent experiments investigated one- and two-dimensional lattice quantum many-body systems at unprecedented sizes, calling for a continuous search of numerical techniques to provide accurate benchmarking and verification of future quantum simulations [1–9]. In particular, Rydberg atoms in optical tweezers are one of the most promising platforms for the study of quantum phase transitions, quantum simulation and computation [10–19]. In the last decades, Monte Carlo and Tensor Networks (TN) algorithms have been employed widely to study quantum many-body systems, and they are routinely used to benchmark quantum simulation results [20–30]. However, Monte Carlo methods are limited by the sign problem [31], while combining accuracy and scalability in simulating high-dimensional systems still represent an open challenge for TN methods [32,33]. Here, we introduce a novel TN variational *Ansatz*, able to encode the area law of quantum many-body states in any spatial dimension by keeping a low algorithmic complexity with respect to standard algorithms (see Fig. 1), thus opening a pathway towards the application of TN to high-dimensional systems. Hereafter, we benchmark this approach against spin models up to sizes of $N = 64 \times 64$, in and out of criticality. Finally, we simulate 2D Rydberg-atom lattices at sizes of up to $\sim$1000, demonstrating the ability of providing the missing benchmarks for very recent quantum simulation experiments [34–37]: nontrivial phase transitions are characterized, in agreement with those experimentally observed in Ref. [34].

In the last three decades, TN have been developed and applied to classically simulate quantum many-body systems, representing the exponentially large wave function with a set of local tensors connected via auxiliary indices with a *bond-dimension* m. The bond dimension m allows us to control the amount of information in the TN, interpolating between mean field ($m = 1$) and the exact but inefficient representation. While for one-dimensional (1D) systems the matrix product states (MPS) are the established TN geometry for equilibrium and out-of-equilibrium problems with open boundary conditions, the development of TN algorithms for 2D or 3D systems

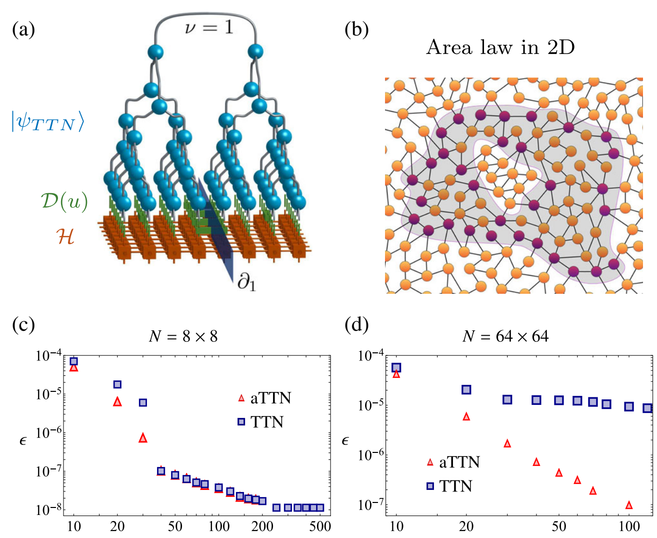

FIG. 1. (a) An aTTN for a 8×8 2D system: The disentanglers in $\mathcal{D}(u)$ are applied to the TTN state $|\psi_{\mathrm{TTN}}\rangle$ across the boundaries ∂_ν of each link ν, in order to fulfill the area law depicted (b) for a sublattice $\mathcal{A}$ (shaded region) and its boundary $\partial\mathcal{A}$ (purple dots). (c),(d) Relative error of the Ising model ground state energy computed with the aTTNs and the TTNs. While for $L = 8$ the precision achieved with the two methods is the same, a clear improvement emerges for $L = 64$.

is still ongoing [38–43]. The most successful TN representations are the projected entangled pair states (PEPS) [44–47] and the tree tensor networks (TTN) [48–51], as well as the multiscale entanglement renormalization *Ansatz* (MERA) [52–54]. The PEPS flourishes for (infinite) 2D systems with open boundary condition and small physical dimension d and MERA provides an efficient representation in critical systems. The TTN offers a very flexible geometry which has proven to be a valid alternative with its particular strong points ranging from applications in gapped 1D systems with periodic boundary conditions [28,50], 2D systems with large local dimension d [24,51] to 3D systems [55].

TNs shall satisfy entanglement bounds under real-space bipartitions, known as area laws, of the *physical states* they represent [39,45,56]. The PEPS is the potentially most powerful TN *Ansatz* and by construction satisfies the area laws of entanglement [56]. However, it suffers from a high algorithmical complexity [typically $\mathcal{O}(m^{10})$ for finite-sized PEPS [46,57,58]] and lacks an exact calculation of expectation values. Indeed, the exact contraction a finite square lattice of the complete PEPS scales exponentially with the system linear dimension L and sophisticated numerical methods shall be introduced to mitigate this unfavorable scaling [58–63]. On the contrary, the MERA in two dimensions is able to calculate expectation values exactly while satisfying area law but suffers from an even higher algorithmical complexity [at least $\mathcal{O}(m^{16})$] [56]. Another well-established approach is to extend the MPS for 2D systems [64]: this approach has a very low algorithmic complexity [$\mathcal{O}(m^3)$], however, it is limited by an exponential scaling of the required bond dimension $m \sim e^{L_k}$ with the system minimal linear size $L_k \equiv \min\{L_x, L_y\}$. As a compromise, TTNs are equally scalable in both system dimensions while still benefiting from a low numerical complexity, $\mathcal{O}(m^4)$ but may fail to satisfy the area law for large systems sizes in higher dimensions [32,65].

Hereafter, we introduce a novel *Ansatz* which augments the TTN and show that is able to encode the area law keeping constant the algorithmic complexity to [$\mathcal{O}(m^4)$] in any physical dimension. As numerically demonstrated hereafter, the augmented tree tensor network (aTTN) allows us to efficiently tackle open challenges in two- and three-dimensional systems at sizes inaccessible before.

Augmented tree tensor network.—The aTTN *Ansatz* $|\psi_{\mathrm{aTTN}}\rangle = \mathcal{D}^\dagger(u)|\psi_{\mathrm{TTN}}\rangle$ is based on a TTN wave function (a binary tree) $|\psi_{\mathrm{TTN}}\rangle \in \bigotimes_i^N \mathcal{H}_i$, with $\mathcal{H}_i = \mathbb{C}^d$, with an additional sparse layer $\mathcal{D}(u) = \prod_k u_k$ of two-site unitary operators $\{u_k\}$ acting on (some of) the physical links of the TTN (see Fig. 1). The additional layer $\mathcal{D}(u)$ contains N_D independent nonoverlapping (i.e., acting on different couples of sites of the lattice $\mathcal{L}$) and thus commuting disentanglers $\{u_k\}$. In this way, $\mathcal{D}(u)$ describes a unitary mapping of the Hamiltonian $\mathcal{H}$ to an auxiliary Hamiltonian $\mathcal{H}_{\mathrm{aux}} = \mathcal{D}(u)\mathcal{H}\mathcal{D}^\dagger(u)$. Each local transformation u_k aims to decouple—or *disentangle* in the spirit of the MERA language [54]—entangled degrees of freedom in the quantum many-body state, that are then trivially included in the TTN layer. As described in the following, $\mathcal{D}(u)$ modifies the TTN in such a way that the aTTN satisfies the area law while keeping the complexity for the optimisation at $\mathcal{O}(m^4)$. Thus, the aTTN overcomes the drawback of the TTN while maintaining its main advantages: (i) the low scaling with the bond dimension m compared to both MERA and PEPS, and (ii) the ability to contract the network exactly. We stress that the aTTN can be applied straighforwardly to a general D-dimensional system. Finally, we notice that the aTTN is effectively a particular subclass of a MERA, where the structure scale invariance is traded for efficiency, as the scale invariance is not necessary to ensure the area law at the tensor structure level. Figure 1(a) reports an illustrative example of an aTTN for a two-dimensional 8×8 system with the $\mathcal{D}(u)$ layer composed by 6 disentanglers u_k (green). Notice that not every physical site j is addressed by a disentangler, a key property for preserving numerical efficiency. Indeed, the disentangler positioning is critical in order to (i) keep an optimal numerical complexity for the optimization and (ii) efficiently encode an area law in the TN.

Area law in aTTN.— Hereafter, we specialize the discussion for the case of a two-dimensional square lattice $\mathcal{L}$ with $N = L \times L$ sites, and $L = 2^n$. Moreover, we consider a binary TTN, where the tree tensors coarse grain neighboring sites for each layer Λ_l alternatingly along the x (for even l) and the y direction (odd l) with l going from $l = 1$ addressing the topmost layer to $l = \log L$ for the lowest layer [Fig. 1(a)]. Each link ν of the tree bipartites the whole system $\mathcal{L}$ into two subsystems $\mathcal{A}^{[\nu]}$ and $\mathcal{B}^{[\nu]}$, separated by the boundary ∂_ν with length γ_ν. The area law implies that the entanglement entropy of the bipartition $S(\mathcal{A}^{[\nu]})$ (or $\mathcal{B}^{[\nu]}$, respectively) scales with γ_ν. Thus, in order to faithfully represent the area law, the bond dimension m_ν of each link ν should scale with $m_\nu \approx e^{c\gamma_\nu}$, where c is a constant factor. This scaling argument implies that for two dimensions the TTN *Ansatz* requires an exponentially large bond dimension m within the topmost layers, for which $\gamma_\nu \sim L$. In conclusion, with increasing L a TTN representation eventually fails to capture area law states' properties as it becomes exponentially inefficient. This necessary exponential scaling of the bond dimension can be prevented by inserting the tensors layer $\mathcal{D}(u)$ that augments the TTN with $N_D = \sum_\nu K_\nu$ disentanglers, where K_ν is the number of disentanglers along the boundary ∂_ν for each link ν. More precisely, each disentangler u_k is positioned such that it acts on one physical site in the subsystems $\mathcal{A}^{[\nu]}$ and the other in subsystems $\mathcal{B}^{[\nu]}$. Thus, each disentangler can maximally assess information in a d^2-dimensional space belonging to two local Hilbert spaces, reducing the entanglement for the TTN up to the order of d^2. As a result, all the K_ν disentanglers support the TTN link ν by disentangling information on the order of $m_{\nu,\mathrm{aux}} \approx (d^2)^{K_\nu}$. Therefore, when applying $\mathcal{D}(u)$, the information assessed by the aTTN for the bipartition defined by each link ν scales with $m_{\nu,\mathrm{eff}} \approx m_{\nu,\mathrm{aux}} m_\nu = d^{2K_\nu + \xi_\nu}$, where we introduced the parameter $\xi_\nu \equiv \log_d m_\nu$ describing the contribution of the TTN bond dimension m_ν. If we now impose $K_\nu \sim \gamma_\nu$, we obtain the exponential scaling required to encode the area law for the two-dimensional aTTN state. Notice that the number of disentanglers $\Gamma_l = \sum_{\nu \in \Lambda_l} K_\nu$ for each layer shall be directly proportional to $\sum_{\nu \in \Lambda_l} \gamma_\nu \sim L$. However, placing exactly L disentanglers for each layer of the tree may lead to an unfavorable, L-dependent scaling of $\mathcal{O}(m^4 d^L)$ for the computational complexity. Thus, a careful balance between the position of the disentanglers and their density has to be found. This balance can be found as when no couple of disentanglers is directly connected by a Hamiltonian interaction term, the algorithmic scaling remains of the order $\mathcal{O}(m^4 d^2)$. Moreover, the area law is still satisfied, removing the disentanglers crossing the boundaries of the bipartitions ∂_ν corresponding to the lower layers of the tree ($l \to \log L$). On the contrary, one shall keep the maximal allowed number of disentanglers (i.e., not connected by Hamiltonian terms) to support the boundaries corresponding to the higher branches ($l \to 1$). Indeed, for $\nu \in \Lambda_l$ with $l \to \log L$, the TTN bond-dimension m_ν is sufficiently large to capture the area law entanglement—or even the complete state—accurately, especially for reasonably small local dimensions d. Instead, the contribution ξ_ν of the TTN is negligibly small for $\nu \in \Lambda_l$ with $l \to 1$ compared to the required exponentially large bond dimension, calling for the support of the disentanglers.

In conclusion, different disentangler configurations $\mathcal{D}(u)$ exist, matching the aforementioned criteria, computational efficiency and the area law. In our numerical simulations, the final resulting precision was not significantly affected by the particularly chosen configuration (for details see Supplemental Material [66]).

Ising model.—We first benchmark the aTTN *Ansatz* against the ordinary TTN via a ground state search on the ferromagnetic 2D Ising model with periodic boundary conditions (BC). We consider a $L \times L$ lattice with $L = \{8, 16, 32, 64\}$ and the Ising Hamiltonian $\mathcal{H} = \sum_{i,j=1}^{L} \sigma^x_{i,j}\sigma^x_{i+1,j} + \sigma^x_{i,j}\sigma^x_{i,j+1} + \sum_{i,j=1}^{L} \sigma^z_{i,j}$, where $\sigma^\gamma_{i,j}$ (with $\gamma \in \{x,y,z\}$) denote the are Pauli matrices acting on the site (i,j). For small system sizes ($L = 8$ and $L = 16$) both the TTN and the aTTN reach the chosen machine precision of `1E-8` with high bond dimension. However, as expected, for larger sizes we find a significant improvement in the precision of the aTTN simulations. Indeed, the different performances become evident for $L = 32$ and $L = 64$, as the aTTN and the TTN converge with increasing bond dimension to different values for the energy Fig. 1 reports the relative error $\epsilon_m = |(\langle\mathcal{H}\rangle_m - E_{ex})/E_{ex}|$ for increasing bond dimension m with respect to the energy E_{ex} obtained by extrapolating the results of the aTTN for $L = 8$ and $L = 64$ (For the $L = 16$, 32 results see Fig. 3 in the Supplemental Material [66]).

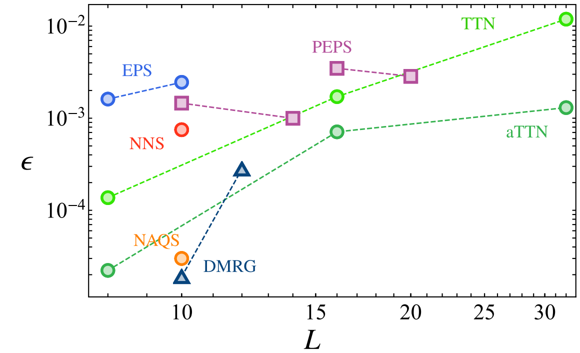

FIG. 2. Relative error ϵ of the 2D Heisenberg ground-state energy as a function of the system linear size L for the TTN, aTTN, NNS [68], NAQS [69], EPS [70], PEPS [58], 2D-DMRG [64] (circles, squares and triangles indicate open BC, periodic BC and cylindrical BC, respectively) each compared with the best available estimates obtained by MC with the same BC (for pbc [22], for obc [58] obtained via ALPS library [75–77]).

Heisenberg model.—We now analyze the more challenging critical antiferromagnetic two dimensional Heisenberg model $\mathcal{H} = \sum_{i,j=1}^{L} \sum_{\gamma \in \{x,y,z\}} \sigma^\gamma_{i,j}\sigma^\gamma_{i+1,j} + \sigma^\gamma_{i,j}\sigma^\gamma_{i,j+1}$, with periodic BC. In Fig. 2 we compare the estimated energy

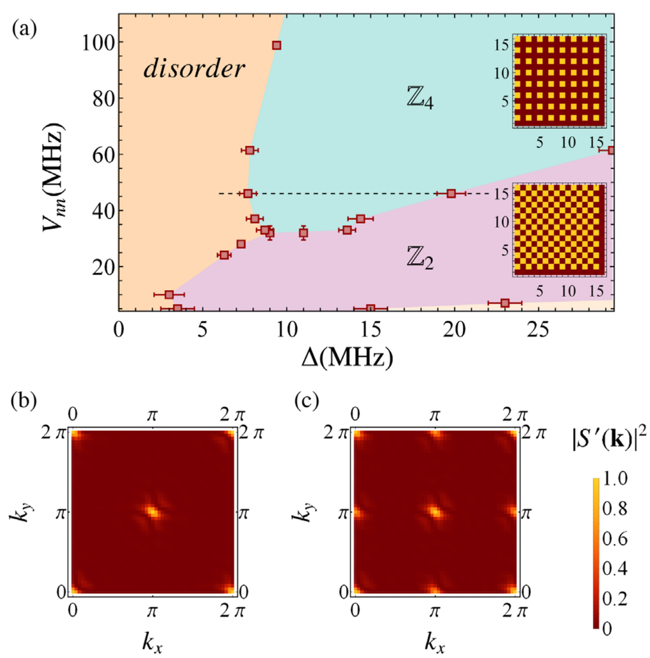

FIG. 3. Up: Phase diagram as a function of the detuning Δ and the nearest-neighbors interaction energy V_{nn}. The disordered phase is characterized by a substantially uniform distribution of the excitations, while in the phases $\mathbb{Z}_2$ and $\mathbb{Z}_4$ the excitations are distributed as shown in the upper ($\mathbb{Z}_4$) and lower ($\mathbb{Z}_2$) insets. Down: Renormalized structure factor $S'(\mathbf{k}) = S(\mathbf{k})/S(\mathbf{0})$ for $V_{nn} = 46$ MHz and (a) $\Delta = 28$ MHz ($\mathbb{Z}_2$ phase) and (b) $\Delta = 12$ MHz ($\mathbb{Z}_4$ phase). Other parameters: $\Omega = 4$ MHz.

density obtained by extrapolating the results from the TTN and the aTTN at $m \to \infty$ with previous results from different variational *Ansätze* obtained by means of ordinary cluster resources [67]. In particular, we plot the relative error obtained by the different tensor network *Ansätze* and the best known results, obtained via quantum Monte Carlo simulations [22]. Differently from the Ising model, we find the aTTN to be more accurate than the TTN even at lower system sizes, such as $L = 8, 16$. Interestingly, the aTTN for $L = 16$ obtains an even more precise ground state energy density compared to most of the alternative variational *Ansätze* at lower finite system size of $L = 10$, such as neural network states (NNS), neural autoregressive quantum state, entangled plaquette states (EPS), or PEPS [58,68–70]. We mention that, while the PEPS is very efficient with its ability to work directly in the thermodynamic limit in describing infinite systems as iPEPS [71,72], the PEPS analysis for finite sizes are, for now, limited to $N = 20 \times 20$ systems. It turns out that for this model a very competitive variational approach is the 2D-DMRG, which outperforms the alternative methods for finite sizes with open or cylindrical BC up to the system size $L = 12$, but struggles with periodic BC and with increasing both system sizes $L \gtrsim 12$ [64]. Finally, we extended our analysis to $L = 32$: In this case no public result is available for periodic BC and thus we estimated the error by extrapolating the value of the finite size scaling of Monte Carlo simulations [22]. In recent works, heavy parallelization over large high performance computing systems have been exploited to study the Heisenberg model with open BC combining the PEPS structure with MC techniques, reaching a precision of $\sim 10^{-4}$ at 32×32 [73,74].

We point out that the here performed aTTN simulations (as well as the TTN simulations) exploit a $U(1)$ symmetry. However, for this model, we could further drastically improve the performance of the aTTN by incorporating the present SU(2) symmetry in the simulation framework [32,78,79].

Interacting Rydberg atoms.—We now present new physical results, on a long-range interacting system by studying the zero-temperature phase diagram of an interacting Rydberg atoms two-dimensional lattice [4], described by the Hamiltonian $\mathcal{H}_{\rm ryd} = \sum_{\mathbf{r}}[(\Omega/2)\sigma^x_{\mathbf{r}} - \Delta n_{\mathbf{r}} + \frac{1}{2}\sum_{\mathbf{s}} V(|\mathbf{r}-\mathbf{s}|) n_{\mathbf{r}} n_{\mathbf{s}}]$, where the Rabi frequency Ω couples the ground $|g\rangle_{\mathbf{r}}$ and the excited Ryderg state $|r\rangle_{\mathbf{r}}$ and $n_{\mathbf{r}} = |r\rangle\langle r|_{\mathbf{r}}$. Δ is the detuning and $V(|\mathbf{r}-\mathbf{s}|) = c_6/|\mathbf{r}-\mathbf{s}|^6$ is the interaction strength between two excited atoms placed at sites $\mathbf{r}$ and $\mathbf{s}$. We keep the interaction terms up to the fourth-nearest neighbor and set the Rabi frequency $\Omega = 4$M Hz, while the interaction parameters refer to ^{87}Rb atoms excited to the state $|70S_{1/2}\rangle$, for which $c_6 = 863$ GHz μm^6.

The interactions limit the maximum excitation density according to the Rydberg blockade radius r^*—the minimum distance at which two atoms can be simultaneously excited—defined by the relation $V(r^*) = \Omega$. The competition between the interactions strength and Δ generates nontrivial phases characterized by regular spatial excitation-density distributions. Figure 3(a) shows the phase diagram of the system as a function of the detuning and the nearest-neighbor interaction energy V_{nn}, obtained via aTTN simulations with $L = 4, 8, 16, 32$ with open BC.

For low values of the detuning Δ, the system exhibits a disordered phase characterized by the absence of excitations while, increasing Δ, excitations are energetically favored and the interactions determine their spatial arrangement. In the limit of $V_{nn} \to 0$, or $a \to \infty$, the atoms are noninteracting and the expectation value $\langle n_{\mathbf{r}}\rangle \to 1$ for $\Delta \ll \Omega$. At larger values of V_{nn}, corresponding to $r^*/\sqrt{2} < a < r^*$, nearest neighbor atoms cannot be simultaneously excited, giving rise to the $\mathbb{Z}_2$ phase [4,80] with a two-degenerate ground state with the excitations distributed in a chess board like configuration, as shown in Fig. 3(a). Nevertheless, the $\mathbb{Z}_2$ disappears at low values of V_{nn} and large detuning, as all the atoms are excited (light orange, right-bottom region of the phase diagram). The spatial distribution of the excitations in the orderded phase is well captured by the peaks of the static structure factor $S(\mathbf{k}) = (1/N^2)\sum_{\mathbf{r},\mathbf{s}} e^{-i\mathbf{k}\cdot(\mathbf{r}-\mathbf{s})}\langle n_{\mathbf{r}} n_{\mathbf{s}}\rangle$. In particular, the phase $\mathbb{Z}_2$ exhibits a peak in (π, π), as shown in Fig. 3(b). The transition from the disordered to the $\mathbb{Z}_2$ phase is a second-order one, as it emerges by computing the second derivative of the energy with respect to Δ (see Supplemental Material [66]). In order to determine the critical line separating the two phases we define the non-local order parameter $O^{(2)}_{\mathbf{r}} = (n_{r_x,r_y} - n_{r_x+1,r_y} - n_{r_x,r_y+1} + n_{r_x+1,r_y+1})/4$ and perform a finite-size scaling analysis of $\langle O^{(2)\dagger}_{\mathbf{r}} O^{(2)}_{\mathbf{r}}\rangle$ vs Δ, where $\langle O^{(2)\dagger}_{\mathbf{r}} O^{(2)}_{\mathbf{r}}\rangle$ is estimated by $S(\pi, \pi)$ [81,82] (see Supplemental Material [66]). By further reducing a, the blockade radius prevents diagonal-adjacent atoms to be excited. As a consequence, each one of the $\mathbb{Z}_2$ ground states breaks into two different states, giving rise to the four-degenerate phase $\mathbb{Z}_4$: In each one of the ground states of this phase, each excited atom is surrounded by atoms in their ground states [see upper inset in Fig. 3(a)]. We observe a second-order phase transition in V_{nn} for $\Delta \simeq 10$ MHz from the $\mathbb{Z}_2$ to the $\mathbb{Z}_4$ phase at $V^c_{nn} = 32 \pm 2.5$ MHz (or equivalently $a = r^*/\sqrt{2}$). The static structure factor exhibits four additional peaks in the points such as $(0, \pi)$ as shown in Fig. 3(c). As in the $\mathbb{Z}_2$ case, a second-order phase transition occurs between the disordered phase to the $\mathbb{Z}_4$ by changing Δ at a fixed V_{nn}. We determine the critical line by introducing the order parameter $O^{(4)}_{\mathbf{r}} = (n_{r_x,r_y} + i n_{r_x+1,r_y} - i n_{r_x,r_y+1} - n_{r_x+1,r_y+1})/4$, defined such that the value of $\langle O^{(4)\dagger}_{\mathbf{r}} O^{(4)}_{\mathbf{r}}\rangle$ equals $S(0, \pi)$ in the $\mathbb{Z}_4$ phase. Remarkably, we find that another second-order phase transition occurs by further increasing Δ, leading the system from the $\mathbb{Z}_4$ to the $\mathbb{Z}_2$ phase. We expect that at larger values of V_{nn} new phases would emerge and accordingly, new phase transitions would occur by changing Δ.

Conclusions.—We have augmented the well-established TTN geometry with a new *Ansatz* which reproduces area law for high dimensional quantum many-body systems. The efficiency of aTTNs allowed us to reach large sizes (32×32) in the study of critical system, going beyond the current possibilities of standard PEPS and DMRG, and therefore set new benchmarks for future numerical simulations [83]. As a first application of aTTNs, we have characterized the phase diagram of two-dimensional Rydberg atoms in optical tweezers, with atoms number of the order of current and near future experiments [2]. Further applications include the study of systems which cannot be studied via Monte Carlo simulations due to the sign problem [31,84], such as Abelian and non-Abelian lattice gauge theories at finite densities [24,55,85–88]. Such an application enables the study of the continuum limit at higher dimensions, paving the way to unveil novel insights into our understanding of the fundamental constituents of our universe [89,90]. Finally, the aTTN *Ansatz* can support known TN algorithms [28,91–96] to investigate nonequilibrium dynamics in open and closed high-dimensional systems, including annealing, quenches, or controlled dynamics.

In conclusion, the aTTN *Ansatz* introduced here provides a novel powerful tool for simulating quantum systems in two or higher dimensions, which, beyond many interesting physical applications will provide benchmark near-future quantum simulations and computations on different platforms, as we have demonstrated for Rydberg atoms in optical tweezers.

This work is partially supported by the Italian PRIN 2017, the INFN project QUANTUM, the Fondazione CARIPARO, the Horizon 2020 research and innovation programme under grant agreement No. 817482 (Quantum Flagship—PASQuanS), the QuantERA projects QTFLAG and QuantHEP, and the DFG project TWITTER. We acknowledge computational resources by CINECA through the Project No. IsC78—EPM2D3, the Cloud Veneto, the BwUniCluster, and by ATOS Bull.

[1] S. de Léséleuc, V. Lienhard, P. Scholl, D. Barredo, S. Weber, N. Lang, H. P. Büchler, T. Lahaye, and A. Browaeys, Observation of a symmetry-protected topological phase of interacting bosons with Rydberg atoms, Science **365**, 775 (2019).

[2] A. Browaeys and T. Lahaye, Many-body physics with individually controlled Rydberg atoms, Nat. Phys. **16**, 132 (2020).

[3] J. Rui, D. Wei, A. Rubio-Abadal, S. Hollerith, J. Zeiher, D. M. Stamper-Kurn, C. Gross, and I. Bloch, A subradiant optical mirror formed by a single structured atomic layer, Nature (London) **583**, 369 (2020).

[4] H. Bernien, S. Schwartz, A. Keesling, H. Levine, A. Omran, H. Pichler, S. Choi, A. S. Zibrov, M. Endres, M. Greiner, V. Vuletić, and M. D. Lukin, Probing many-body dynamics on a 51-atom quantum simulator, Nature (London) **551**, 579 (2017).

[5] P. Schauß, M. Cheneau, M. Endres, T. Fukuhara, S. Hild, A. Omran, T. Pohl, C. Gross, S. Kuhr, and I. Bloch, Observation of spatially ordered structures in a two-dimensional Rydberg gas, Nature (London) **491**, 87 (2012).

[6] A. Elben, B. Vermersch, R. van Bijnen, C. Kokail, T. Brydges, C. Maier, M. K. Joshi, R. Blatt, C. F. Roos, and P. Zoller, Cross-Platform Verification of Intermediate Scale Quantum Devices, Phys. Rev. Lett. **124**, 010504 (2020).

[7] T. Olsacher, L. Postler, P. Schindler, T. Monz, P. Zoller, and L. M. Sieberer, Scalable and parallel tweezer gates for quantum computing with long ion strings, PRX Quantum **1**, 020316 (2020).

[8] C. Kokail, C. Maier, R. van Bijnen, T. Brydges, M. K. Joshi, P. Jurcevic, C. A. Muschik, P. Silvi, R. Blatt, C. F. Roos, and P. Zoller, Self-verifying variational quantum simulation of lattice models, Nature (London) **569**, 355 (2019).

[9] A. Celi, B. Vermersch, O. Viyuela, H. Pichler, M. D. Lukin, and P. Zoller, Emerging Two-Dimensional Gauge Theories in Rydberg Configurable Arrays, Phys. Rev. X **10**, 021057 (2020).

[10] H. Labuhn, D. Barredo, S. Ravets, S. de Léséleuc, T. Macrì, T. Lahaye, and A. Browaeys, Tunable two-dimensional arrays of single Rydberg atoms for realizing quantum Ising models, Nature (London) **534**, 667 (2016).

[11] P. Schauss, Quantum simulation of transverse Ising models with Rydberg atoms, Quantum Sci. Technol. **3**, 023001 (2018).

[12] S. Notarnicola, M. Collura, and S. Montangero, Real-time-dynamics quantum simulation of (1+1)-dimensional lattice QED with Rydberg atoms, Phys. Rev. Research **2**, 013288 (2020).

[13] F. M. Surace, P. P. Mazza, G. Giudici, A. Lerose, A. Gambassi, and M. Dalmonte, Lattice Gauge Theories and String Dynamics in Rydberg Atom Quantum Simulators, Phys. Rev. X **10**, 021041 (2020).

[14] D. Barredo, V. Lienhard, S. de Léséleuc, T. Lahaye, and A. Browaeys, Synthetic three-dimensional atomic structures assembled atom by atom, Nature (London) **561**, 79 (2018).

[15] D. Barredo, V. Lienhard, P. Scholl, S. de Léséleuc, T. Boulier, A. Browaeys, and T. Lahaye, Three-Dimensional Trapping of Individual Rydberg Atoms in Ponderomotive Bottle Beam Traps, Phys. Rev. Lett. **124**, 023201 (2020).

[16] V. Lienhard, S. de Léséleuc, D. Barredo, T. Lahaye, A. Browaeys, M. Schuler, L.-P. Henry, and A. M. Läuchli, Observing the Space- and Time-Dependent Growth of Correlations in Dynamically Tuned Synthetic Ising Models with Antiferromagnetic Interactions, Phys. Rev. X **8**, 021070 (2018).

[17] A. Omran *et al.*, Generation and manipulation of Schrödinger cat states in Rydberg atom arrays, Science **365**, 570 (2019).

[18] H. Levine *et al.*, Parallel Implementation of High-Fidelity Multiqubit Gates with Neutral Atoms, Phys. Rev. Lett. **123**, 170503 (2019).

[19] M. Morgado and S. Whitlock, Quantum simulation and computing with Rydberg-interacting qubits, arXiv:2011.03031.

[20] J. Kolorenč and L. Mitas, Applications of quantum Monte Carlo methods in condensed systems, Rep. Prog. Phys. **74**, 026502 (2011).

[21] P. H. Acioli, Review of quantum Monte Carlo methods and their applications, J. Mol. Struct. Theochem **394**, 75 (1997).

[22] A. W. Sandvik, Finite-size scaling of the ground-state parameters of the two-dimensional Heisenberg model, Phys. Rev. B **56**, 11678 (1997).

[23] S. Montangero, *Introduction to Tensor Network Methods* (Springer International Publishing, Cham, 2018).

[24] T. Felser, P. Silvi, M. Collura, and S. Montangero, Two-dimensional quantum-link lattice Quantum Electrodynamics at finite density, arXiv:1911.09693.

[25] R. Orús, Tensor networks for complex quantum systems, Nat. Rev. Phys. **1**, 538 (2019).

[26] F. Arute *et al.*, Quantum supremacy using a programmable superconducting processor, Nature (London) **574**, 505 (2019).

[27] Bañuls *et al.*, Simulating lattice gauge theories within quantum technologies, Eur. Phys. J. D **74**, 165 (2020).

[28] L. Kohn, P. Silvi, M. Gerster, M. Keck, R. Fazio, G. E. Santoro, and S. Montangero, Superfluid-to-Mott transition in a Bose-Hubbard ring: Persistent currents and defect formation, Phys. Rev. A **101**, 023617 (2020).

[29] E. Macaluso, T. Comparin, R. O. Umucalilar, M. Gerster, S. Montangero, M. Rizzi, and I. Carusotto, Charge and statistics of lattice quasiholes from density measurements: A tree tensor network study, Phys. Rev. Research **2**, 013145 (2020).

[30] P. Emonts, M. C. Bañuls, I. Cirac, and E. Zohar, Variational Monte Carlo simulation with tensor networks of a pure $\mathbb{Z}_3$ gauge theory in (2+1)D, Phys. Rev. D **102**, 074501 (2020).

[31] M. Troyer and U.-J. Wiese, Computational Complexity and Fundamental Limitations to Fermionic Quantum Monte Carlo Simulations, Phys. Rev. Lett. **94**, 170201 (2005).

[32] P. Silvi, F. Tschirsich, M. Gerster, J. Jünemann, D. Jaschke, M. Rizzi, and S. Montangero, The Tensor Networks Anthology: Simulation techniques for many-body quantum lattice systems, SciPost Phys. Lect. Notes **8**, 3 (2019).

[33] S.-J. Ran, E. Tirrito, C. Peng, X. Chen, L. Tagliacozzo, G. Su, and M. Lewenstein, *Two-dimensional tensor networks and contraction algorithms, in Tensor Network Contractions: Methods and Applications to Quantum Many-Body Systems* (Springer International Publishing, Cham, 2020), pp. 63–86.

[34] S. Ebadi *et al.*, Quantum phases of matter on a 256-atom programmable quantum simulator, arXiv:2012.12281.

[35] D. Bluvstein *et al.*, Controlling many-body dynamics with driven quantum scars in Rydberg atom arrays, arXiv:2012.12276.

[36] P. Scholl*et al.*, Programmable quantum simulation of 2D antiferromagnets with hundreds of Rydberg atoms, arXiv:2012.12268.

[37] R. Samajdar, W. W. Ho, H. Pichler, M. D. Lukin, and S. Sachdev, Complex Density Wave Orders and Quantum Phase Transitions in a Model of Square-Lattice Rydberg Atom Arrays, Phys. Rev. Lett. **124**, 103601 (2020).

[38] S. Östlund and S. Rommer, Thermodynamic Limit of Density Matrix Renormalization, Phys. Rev. Lett. **75**, 3537 (1995).

[39] F. Verstraete and J. I. Cirac, Matrix product states represent ground states faithfully, Phys. Rev. B **73**, 094423 (2006).

[40] S. R. White, Density matrix formulation for quantum renormalization groups, Phys. Rev. Lett. **69**, 2863 (1992).

[41] U. Schollwöck, The density-matrix renormalization group in the age of matrix product states, Ann. Phys. (Amsterdam) **326**, 96 (2011).

[42] S. R. White and A. E. Feiguin, Real-Time Evolution Using the Density Matrix Renormalization Group, Phys. Rev. Lett. **93**, 076401 (2004).

[43] G. Vidal, Efficient Classical Simulation of Slightly Entangled Quantum Computations, Phys. Rev. Lett. **91**, 147902 (2003).

[44] F. Verstraete and J. I. Cirac, Valence-bond states for quantum computation, Phys. Rev. A **70**, 060302(R) (2004).

[45] F. Verstraete, M. M. Wolf, D. Perez-Garcia, and J. I. Cirac, Criticality, the Area Law, and the Computational Power of Projected Entangled Pair States, Phys. Rev. Lett. **96**, 220601 (2006).

[46] R. Orús, A practical introduction to tensor networks: Matrix product states and projected entangled pair states, Ann. Phys. (Amsterdam) **349**, 117 (2014).

[47] F. Verstraete and J. I. Cirac, Renormalization algorithms for Quantum-Many Body Systems in two and higher dimensions, arXiv:cond-mat/0407066.

[48] Y.-Y. Shi, L.-M. Duan, and G. Vidal, Classical simulation of quantum many-body systems with a tree tensor network, Phys. Rev. A **74**, 022320 (2006).

[49] P. Silvi, V. Giovannetti, S. Montangero, M. Rizzi, J. I. Cirac, and R. Fazio, Homogeneous binary trees as ground states of quantum critical Hamiltonians, Phys. Rev. A **81**, 062335 (2010).

[50] M. Gerster, P. Silvi, M. Rizzi, R. Fazio, T. Calarco, and S. Montangero, Unconstrained tree tensor network: An adaptive gauge picture for enhanced performance, Phys. Rev. B **90**, 125154 (2014).

[51] M. Gerster, M. Rizzi, P. Silvi, M. Dalmonte, and S. Montangero, Fractional quantum Hall effect in the interacting Hofstadter model via tensor networks, Phys. Rev. B **96**, 195123 (2017).

[52] G. Vidal, Entanglement Renormalization, Phys. Rev. Lett. **99**, 220405 (2007).

[53] G. Evenbly and G. Vidal, Entanglement Renormalization in Two Spatial Dimensions, Phys. Rev. Lett. **102**, 180406 (2009).

[54] G. Evenbly and G. Vidal, Algorithms for entanglement renormalization, Phys. Rev. B **79**, 144108 (2009).

[55] G. Magnifico, T. Felser, P. Silvi, and S. Montangero, Lattice Quantum Electrodynamics in (3+1)-dimensions at finite density with Tensor Networks, arXiv:2011.10658.

[56] J. Eisert, M. Cramer, and M. B. Plenio, Colloquium: Area laws for the entanglement entropy, Rev. Mod. Phys. **82**, 277 (2010).

[57] P. Czarnik and J. Dziarmaga, Variational approach to projected entangled pair states at finite temperature, Phys. Rev. B **92**, 035152 (2015).

[58] M. Lubasch, J. I. Cirac, and M.-C. Bañuls, Algorithms for finite projected entangled pair states, Phys. Rev. B **90**, 064425 (2014).

[59] J. Haferkamp, D. Hangleiter, J. Eisert, and M. Gluza, Contracting projected entangled pair states is average-case hard, Phys. Rev. Research **2**, 013010 (2020).

[60] S.-J. Dong, C. Wang, Y. Han, G.-c. Guo, and L. He, Gradient optimization of fermionic projected entangled pair states on directed lattices, Phys. Rev. B **99**, 195153 (2019).

[61] H. Ueda, K. Okunishi, S. Yunoki, and T. Nishino, Corner transfer matrix renormalization group analysis of the two-dimensional dodecahedron model, Phys. Rev. E **102**, 032130 (2020).

[62] T. Nishino and K. Okunishi, Corner transfer matrix renormalization group method, J. Phys. Soc. Jpn. **65**, 891 (1996).

[63] N. Schuch, M. M. Wolf, F. Verstraete, and J. I. Cirac, Computational Complexity of Projected Entangled Pair States, Phys. Rev. Lett. **98**, 140506 (2007).

[64] E. Stoudenmire and S. R. White, Studying two-dimensional systems with the density matrix renormalization group, Annu. Rev. Condens. Matter Phys. **3**, 111 (2012).

[65] A. J. Ferris, Area law and real-space renormalization, Phys. Rev. B **87**, 125139 (2013).

[66] See Supplemental Material at http://link.aps.org/supplemental/10.1103/PhysRevLett.126.170603 for a more technical description of the aTTN Ansatz and a deeper analysis of the 2D quantum Ising model, critical Heisemberg and Rydberg atom lattice simulations.

[67] The simulations presented here have been performed on a single cluster node.

[68] G. Carleo and M. Troyer, Solving the quantum many-body problem with artificial neural networks, Science **355**, 602 (2017).

[69] O. Sharir, Y. Levine, N. Wies, G. Carleo, and A. Shashua, Deep Autoregressive Models for the Efficient Variational Simulation of Many-Body Quantum Systems, Phys. Rev. Lett. **124**, 020503 (2020).

[70] F. Mezzacapo, N. Schuch, M. Boninsegni, and J. I. Cirac, Ground-state properties of quantum many-body systems: entangled-plaquette states and variational Monte Carlo, New J. Phys. **11**, 083026 (2009).

[71] J. Jordan, R. Orús, G. Vidal, F. Verstraete, and J. I. Cirac, Classical Simulation of Infinite-Size Quantum Lattice Systems in Two Spatial Dimensions, Phys. Rev. Lett. **101**, 250602 (2008).

[72] R. Orús and G. Vidal, Simulation of two-dimensional quantum systems on an infinite lattice revisited: Corner transfer matrix for tensor contraction, Phys. Rev. B **80**, 094403 (2009).

[73] L. He, H. An, C. Yang, F. Wang, J. Chen, C. Wang, W. Liang, S. Dong, Q. Sun, W. Han, W. Liu, Y. Han, and W. Yao, PEPS++: Towards extreme-scale simulations of strongly correlated quantum many-particle models on sunway taihulight, IEEE Trans. Parallel Distributed Syst. **29**, 2838 (2018).

[74] W.-Y. Liu, Y.-Z. Huang, S.-S. Gong, and Z.-C. Gu, Accurate simulation for finite projected entangled pair states in two dimensions, arXiv:1908.09359.

[75] S. Todo and K. Kato, Cluster Algorithms for General- S Quantum Spin Systems, Phys. Rev. Lett. **87**, 047203 (2001).

[76] A. Albuquerque, F. Alet, P. Corboz, P. Dayal, A. Feiguin, S. Fuchs, L. Gamper, E. Gull, S. Gürtler, A. Honecker *et al.*, The ALPS project release 1.3: Open-source software for strongly correlated systems, J. Magn. Magn. Mater. **310**, 1187 (2007).

[77] B. Bauer *et al.*, The ALPS project release 2.0: open source software for strongly correlated systems, J. Stat. Mech. (2011) P05001.

[78] S. Singh and G. Vidal, Global symmetries in tensor network states: Symmetric tensors versus minimal bond dimension, Phys. Rev. B **88**, 115147 (2013).

[79] S. Singh, Tensor network states and algorithms in the presence of abelian and non-abelian symmetries, arXiv:1203.2222.

[80] P. Schauß, J. Zeiher, T. Fukuhara, S. Hild, M. Cheneau, T. Macrì, T. Pohl, I. Bloch, and C. Gross, Crystallization in Ising quantum magnets, Science **347**, 1455 (2015).

[81] K. Binder, Finite size scaling analysis of ising model block distribution functions, Z. Phys. B **43**, 119 (1981).

[82] G. Giudici, A. Angelone, G. Magnifico, Z. Zeng, G. Giudice, T. Mendes-Santos, and M. Dalmonte, Diagnosing Potts criticality and two-stage melting in one-dimensional hard-core boson models, Phys. Rev. B **99**, 094434 (2019).

[83] For a discussion concerning the possibility to improve the efficiency our simulations see the Supplemental Material [66] and Refs. [97,98].

[84] M. C. Bañuls and K. Cichy, Review on novel methods for lattice gauge theories, Rep. Prog. Phys. **83**, 024401 (2020).

[85] M. C. Bañuls, R. Blatt, J. Catani, A. Celi, J. I. Cirac, M. Dalmonte, L. Fallani, K. Jansen, M. Lewenstein, S. Montangero, C. A. Muschik, B. Reznik, E. Rico, L. Tagliacozzo, K. V. Acoleyen, F. Verstraete, U. J. Wiese, M. Wingate, J. Zakrzewski, and P. Zoller, Simulating lattice gauge theories within quantum technologies, arXiv:1911.00003.

[86] M. Dalmonte and S. Montangero, Lattice gauge theory simulations in the quantum information era, Contemp. Phys. **57**, 388 (2016).

[87] T. M. R. Byrnes, P. Sriganesh, R. J. Bursill, and C. J. Hamer, Density matrix renormalization group approach to the massive Schwinger model, Phys. Rev. D **66**, 013002 (2002).

[88] P. Silvi, E. Rico, T. Calarco, and S. Montangero, Lattice gauge tensor networks, New J. Phys. **16**, 103015 (2014).

[89] I. J. R. Aitchison and A. J. G. Hey, *Gauge Theories in Particle Physics: A Practical Introduction. Vol. 1: From Relativistic Quantum Mechanics to QED* (CRC Press, Bristol, UK, 2003).

[90] T. Cheng and L. Li, *Gauge Theory of Elementary Particle Physics* (Oxford University Press, New York, 2006).

[91] M. Rizzi, S. Montangero, and G. Vidal, Simulation of time evolution with multiscale entanglement renormalization ansatz, Phys. Rev. A **77**, 052328 (2008).

[92] L. Arceci, P. Silvi, and S. Montangero, Entanglement of formation of mixed many-body quantum states via Tree Tensor Operators, arXiv:2011.01247.

[93] J. Haegeman, J. I. Cirac, T. J. Osborne, I. Pižorn, H. Verschelde, and F. Verstraete, Time-Dependent Variational

Principle for Quantum Lattices, Phys. Rev. Lett. **107**, 070601 (2011).

[94] J. Haegeman, C. Lubich, I. Oseledets, B. Vandereycken, and F. Verstraete, Unifying time evolution and optimization with matrix product states, Phys. Rev. B **94**, 165116 (2016).

[95] C. Lubich, I. V. Oseledets, and B. Vandereycken, Time integration of tensor trains, SIAM J. Numer. Anal. **53**, 917 (2015).

[96] D. Bauernfeind and M. Aichhorn, Time dependent variational principle for tree Tensor Networks, SciPost Phys. **8**, 24 (2020).

[97] N. Ossi, L. Bitton, D. B. Gutman, and A. Frydman, Zero-bias anomaly in a two-dimensional granular insulator, Phys. Rev. B **87**, 115137 (2013).

[98] A. Milsted, M. Ganahl, S. Leichenauer, J. Hidary, and G. Vidal, TensorNetwork on TensorFlow: A spin chain application using tree Tensor Networks, arXiv:1905.01331.